crystals

MDPI

*Communication*

# R-Phase Transformation Evolution in NiTi SMA Wires Studied via the Internal Friction Technique

**Yuhao Xu [1,2], Junlan Chen [1,2], Xinggang Wang [1,2], Meng Sun [1,*], Xianping Wang [1] and Weibin Jiang [1,*]**

[1] Key Laboratory of Materials Physics, Institute of Solid State Physics, Hefei Institutes of Physical Science, Chinese Academy of Sciences, Hefei 230031, China
[2] University of Science and Technology of China, Hefei 230026, China
* Correspondence: mengsun@issp.ac.cn (M.S.); wbjiang@issp.ac.cn (W.J.); Tel.: +86-18955191689 (W.J.)

**Abstract:** The specific damping capacity variation of heat-treated NiTi was observed during a pseudoelasticity test. The detailed B2 → R-phase transformation process in cold-drawn NiTi wires undergoing middle-temperature aging was studied via X-ray diffraction, transmission electron microscope, and internal friction technique. Results show that, as aging time increased at 450 °C, the dynamic phase transition splitting from B2 → R to B2 → $R_1$ and B2 → $R_2$ became evident. However, such a splitting process was not observed for the sample after aging at 400 °C. The reason for R-phase generation is attributed to non-uniformly distributed stress fields. The splitting of the internal friction peak, in conjunction with high-resolution transmission electron microscope and mechanic results, suggests a substantial occurrence of short-range segregation of Ni atoms in the B2-NiTi matrix. Furthermore, the specific damping capacity (SDC) exhibits a gradual increase with prolonged annealing time. Specifically, the sample with significant dynamic phase transition splitting reaches an SDC value of 0.60.

**Keywords:** NiTi alloy; phase transformation; R phase; microstructure; variant; internal friction



**Citation:** Xu, Y.; Chen, J.; Wang, X.; Sun, M.; Wang, X.; Jiang, W. R-Phase Transformation Evolution in NiTi SMA Wires Studied via the Internal Friction Technique. *Crystals* **2024**, *14*, 476. https://doi.org/10.3390/cryst14050476

Academic Editors: Marek Sroka and Shouxun Ji

Received: 18 April 2024
Revised: 6 May 2024
Accepted: 16 May 2024
Published: 18 May 2024



## 1. Introduction

Near-equiatomic NiTi shape memory alloys (SMAs), due to their unique properties, have been widely used in medical implants [1–4], the aerospace industry [5], and damping applications [6,7]. The R phase, a pivotal transitional state in the transformation pathway from the B2 parent phase to the B19′ martensite in NiTi alloy [8], has a significant impact on the excellent pseudoelastic performance and can be introduced by severe cold working and subsequent thermal treatment. Therefore, investigating the impact of the R-phase structure in near-equiatomic NiTi alloys on their properties holds significant importance for shock absorbers.

There are numerous research reports on the generation of the R phase. Wang et al. provide a summary of R-phase studies [9]. They specifically emphasize that the introduction of the R phase through low-temperature long-term aging (aging at 250 °C for 24 h) requires the inhibition of the transformation of the B19′ phase by nanoprecipitate $Ni_4Ti_3$, while the mechanism for generating the $R_2$ variant is the non-uniformity of nanoprecipitate $Ni_4Ti_3$ density within the grains and near the grain boundaries. By combining atomic-resolution transmission electron microscopy and geometrical phase analysis (GPA), Wim and Dominique confirmed that the introduction of the R phase compensates for the elastic strain introduced by the precipitate [10]. Khalil-Allafi et al. [11] reported the phase transformation of a Ni-rich NiTi subjected to 500 °C stress assisted aging. Interestingly, with the extension of aging time, the peak temperature of phase transition gradually approaches. Tirry and Schryvers [12] used high-resolution transmission electron microscopy (HRTEM) and image-processing techniques to measure the strain fields around $Ni_4Ti_3$ precipitates. This study demonstrated that the maximum expansive strain is not located at the interface

of the precipitate, but increased with the size of the precipitate, which directly proved the concept of R-phase nucleation near precipitates due to local lattice strains.

However, some articles have recently reported the phase transition phenomenon of the R phase without $Ni_4Ti_3$ nanoprecipitates. Song et al. [13] reported cases of R-phase transformation without the introduction of nanoprecipitates of $Ni_4Ti_3$ and fabricated an alloy with ultra-high damping performance, which was subjected to low-temperature aging after insufficient annealing from severe deformation. By using molecular dynamics (MD) and GPA methods, Huo et al. [14] extensively discussed the mechanism of R-phase generation in low-temperature (250 °C) aged NiTi alloys. They argued that when strain fluctuations exceed ±3%, the R phase will form, and with increasing aging time, the temperature window widens. It is noteworthy that, in their study, the most influential $Ni_4Ti_3$ was not observed.

The same question arises in mid-temperature aging: Can severely plastically deformed NiTi alloys generate the R phase and its variants without the presence of $Ni_4Ti_3$? However, it seems widely believed that mid-temperature aging introduces precipitation. Bojda et al. reported the precipitation of $Ni_4Ti_3$ and its variants in Ni-rich NiTi subjected to 500 °C−1 h [15]. Jiang et al. directly observed a substantial amount of $Ni_4Ti_3$ in NiTi samples annealed at temperatures of 573 K (300 °C), 723 K (450 °C), and 873 K (600 °C) for 2 h [16]. On the other hand, Urbina et al. [17] have conducted an investigation of NiTi subjected to aging from 450 °C to 525 °C, and found that a substantial density of dislocations can be preserved until 500 °C, facilitating the formation of a fully developed R phase. Conversely, when the aging temperature surpasses 500 °C, the R phase becomes undetectable. Thus, these existing studies suggest that temperature and time play a crucial role in the R-phase transition.

DSC is widely employed in the characterization of phase transformations in NiTi alloys. However, its inherently rapid heating/cooling rates may obscure some of the transformation information related to the R phase. The IF technique is sensitive to the martensitic transformation with a lower cooling rate. In this study, we focused on cold-drawn near-equiatomic NiTi wires, which were subjected to mid-temperature aging to achieve excellent pseudoelasticity. Subsequently, we investigated the phase transformation behavior of different heat-treated samples using the IF technique. Our findings revealed that the phase transformation is highly sensitive to the pre-heat treatment process, and the phase transition IF peak exhibits splitting. Finally, we discussed these phenomena by integrating transmission electron microscopy results.

## 2. Materials and Methods

### *2.1. Materials and Heat-Treatment*

Commercial 80% area reduction cold-drawn NiTi wire with a diameter of 0.6 mm was received from Jiangsu Peier Technology at the nominal chemical composition of $Ni_{50.45}Ti_{49.55}$ (.at%). To obtain better pseudoelastic properties, the materials underwent heat treatment at 400 °C, 450 °C, and 500 °C for 10, 20, 40, and 60 min in a tubular furnace under an argon atmosphere, and then quenched in water (~18 °C).

### *2.2. Tensile Properties Test and Hysteresis Loop Test*

Tensile testing of NiTi wire was conducted on an Instron 9657 machine for both the as-received sample and those subjected to different heat treatments. Tests were performed at room temperature, with the 100 mm length between clamps. The strain rate during tensile testing was set at $5 \times 10^{-3}$ $s^{-1}$.

Hysteresis loop testing of NiTi wire was conducted on the Instron 9657 machine for heat-treated samples at room temperature (~20 °C). The total length of the wire samples tested was 100 mm. The strain rate for tensile loading in the positive direction was set at 0.05% per second, while for the reverse loading, it was set at −0.05% per second. A strain level of 6.0% was set for tensile loading, and upon reaching this strain level during positive

loading, the loading direction was reversed for reverse loading until the final load value reached 0 N.

All mechanical tests on the samples were repeated at least three times, with representative results exhibiting typical characteristics being selected.

### 2.3. X-ray Diffraction

The phase composition of the samples was analyzed using an X'Pert powder X-ray diffractometer (X'Pert$^3$ MRD, manufactured by Malvern Panalytical, Alemlo, The Netherland) (CuK$\alpha$, $\lambda$ = 1.5418 Å). Fast sweeps were performed over 10–90° in 0.032° increments, and fine sweeps were performed over the range 36–48° in 0.016° increments.

### 2.4. TEM Characterization

The microstructures of the samples were characterized by TEM (FEI Tecnai G2 F20, manufactured by FEI, Columbia, Maryland). The accelerating voltage was 200 kV. Before testing, NiTi materials undergo preprocessing, with a focus on selecting NiTi wire samples based on their circular cross-sections. The initial step entails reducing the thickness of the samples through grinding. Given that the sample diameter was less than 3 mm, the samples were initially sanded with sandpaper down to 100 μm. They were then adhered to a Mo ring using AB glue and gently polished further to 50 μm. To achieve an ultra-thin region suitable for TEM, ion thinning was employed. At the onset of this process, the ion beam voltage was set at 5 kV. Upon the emergence of minute pores, the voltage was lowered to 3.5 kV to meticulously continue the thinning until a sample meeting the TEM standard was attained.

### 2.5. Internal Friction

IF measurements were accomplished using an automatic inverted torsion pendulum apparatus (MFIFA, Hefei, China). The wire samples were clamped at both ends, and the wire length between clamps was about 40 mm. During the IF measurement, the sample was periodically twisted at the upper end, while the lower end was fixed. The IF value $Q^{-1}$ was determined by a direct measurement of the phase angle, $\phi$, by which the strain lags behind the stress. The forced amplitude on the sample is $20 \times 10^{-6}$ and the torsion frequency were set to 0.5 Hz, 1.0 Hz, and 2.0 Hz. Test began at room temperature (RT), and the sample was heated and kept at 90 °C for 10 min. Then, the temperature was lowered to about −70 °C. The cooling rate was 2 °C/min.

## 3. Results and Discussion

### 3.1. Tensile Properties

Figure 1a shows the mechanical properties of the as-received sample. The tensile strength of this cold-worked sample is up to 1900 MPa, but the elongation is low and the pseudoelastic plateau did not appear in the curve. Neither a distinct yielding stage nor a stress plateau attributable to pseudoelasticity is observed. The sample fractures at the point of tensile strength, suggesting that a significant amount of substructure or internal stress has been introduced into the cold-drawn NiTi alloy, leading to the fracture of the wire without necking.

In contrast, Figure 1b presents the mechanical curves of the samples with different heat treatment processes; all samples exhibit distinct stress plateaus indicative of pseudoelasticity. Notably, these heat-treated samples show a decreasing trend in ultimate tensile strength (UTS) compared to the as-received material. The 400 °C–10 min sample demonstrates the closest resemblance to the as-received samples in terms of UTS. The UTS of the samples only decreased by 10 MPa (from 1900 MPa to 1890 MPa), whereas its total elongation was significantly enhanced. On the other hand, the rapid middle-temperature aging (mid-temperature aging) method led to the emergence of a stress plateau in the samples, with a strain value of approximately 7% to the right of this plateau. It can be inferred that the introduction of this stress plateau has broadened the total elongation

compared to the as-received samples. Interestingly, although the diameter of the wire samples precludes precise measurement of the elastic modulus using an extensometer, a distinct elastic modulus was observed on either side of the stress plateau. This is attributed to stress-induced phase transformation, a phenomenon that has been extensively studied in superelastic NiTi alloys.

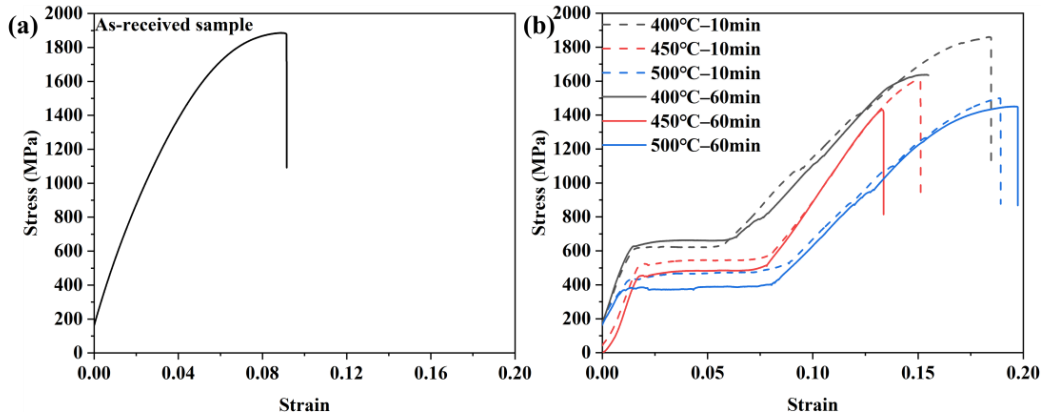


**Figure 1.** Mechanical properties for different heat-treated samples: (**a**) as-received samples and (**b**) samples subjected to various heat treatment processes with aging temperatures of 400 °C, 450 °C, and 500 °C, and durations of 10 and 60 min.

Increasing the heat treatment temperature results in a marked decrease in the pseudoelastic plateau, and extending the holding time also leads to a rapid decline of the plateau for samples treated at 450 °C and 500 °C. The samples treated at 400 °C with extended time maintain a nearly constant platform stress of around 650 MPa. The reversible strain of the samples increases gradually, with the holding time exerting a relatively minor influence. We speculate that the heat treatment induces material recovery, leading to the partial elimination of substructures such as dislocations and internal stresses. It is noteworthy that all samples still do not exhibit necking phenomena; instead, they fracture at the UTS position. However, these speculations require further experimental verification.

Nevertheless, the tensile experiments can be regarded as preliminary experiments. We have observed potential pseudoelastic properties of the samples in the temperature range of 400–500 °C during heat treatment.

### *3.2. Pseudoelasticity Properties and Specific Damping Capacity*

Figure 2a–c presents the hysteresis curve results of NiTi subjected to different heat treatments, and Figure 2d presents the calculated results of the specific damping capacity (SDC). Since the as-received samples in Section 3.1 did not exhibit distinct pseudoelastic curve characteristics, they were not tested. Additionally, all samples in the 500 °C group exhibited varying degrees of bending during the return loading process; therefore, SDC numerical calculations were not performed for this temperature group and we will not discuss this temperature further.

Figure 2a,b illustrate typical pseudoelastic flag-type curves of NiTi alloy, which, owing to their large envelope area, possess significant energy dissipation capabilities. The hysteresis curves depicted in Figure 2a,b exhibit distinct upper and lower stress plateaus, which are the result of stress-induced phase transformation and are typical characteristics of pseudoelasticity in NiTi. Lorène et al. conducted in situ testing using synchrotron X-ray radiation diffraction (SXRD) to investigate this process and demonstrated the existence of the B2-R-B19′ phase transformation pathway during loading. However, only a single B2 phase diffraction peak was observed during the unloading process [18].

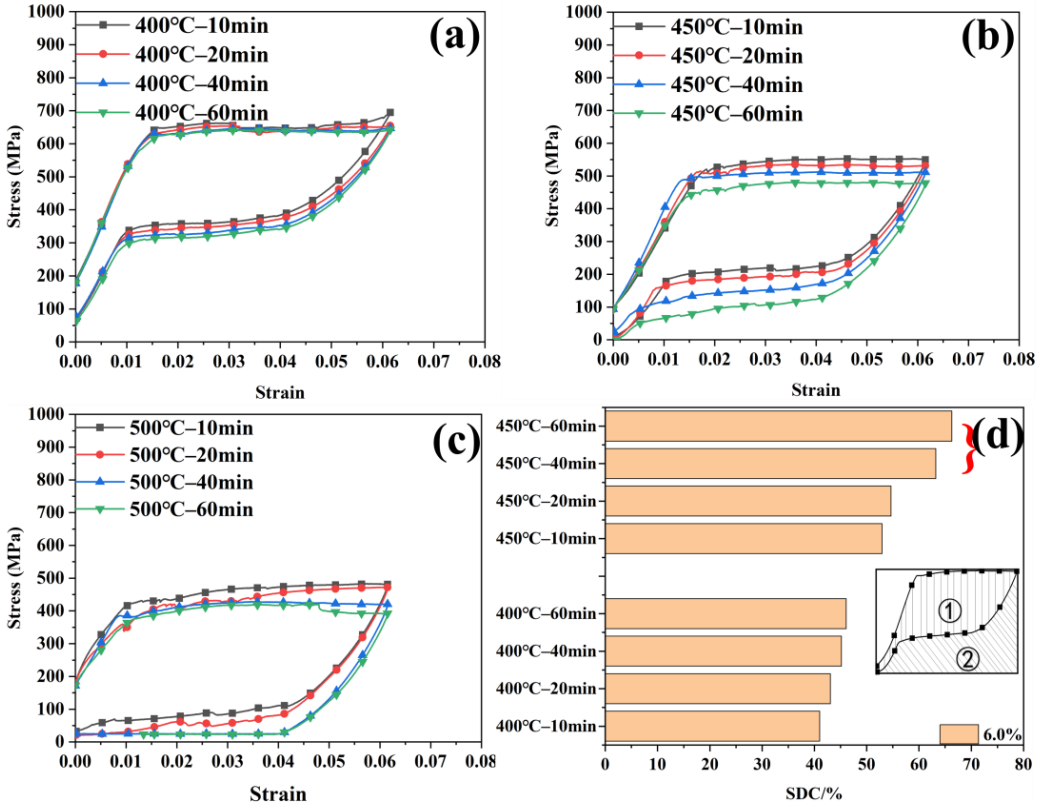


**Figure 2.** Hysteresis loop for different heat-treated samples subjected to (**a**) 400 °C, (**b**) 450 °C, (**c**) 500 °C. (**d**)calculated Specific Damping Capacity (SDC) of 400 °C and 450 °C samples. An inset was given in (**d**), where region ① is the envelope area of the hysteresis curve, while region ② is the shaded area of the unloading curve.

Comparing Figure 2a,b, significant differences can be observed in both the upper and lower stress plateaus. Figure 2a shows that the upper stress plateau of the samples treated at 400 °C remains almost unchanged at 650 MPa, while the stress value of the lower stress plateau exhibits a slight decrease with prolonged annealing time, with a decrease of 50 MPa (from 350 MPa to 300 MPa). However, in Figure 2b, for samples treated at 450 °C, the decrease in the upper stress plateau is 100 MPa (from 550 MPa to 450 MPa), and the lower stress plateau experiences a drastic decrease (from 200 MPa to 100 MPa), particularly for samples annealed for 40 min and 60 min, where the changes are most pronounced.

For a more in-depth discussion of this phenomenon, the SDC calculation equation (Equation (1)) was employed to calculate the curves in Figure 2a,b. The specific calculation results are presented in Figure 2d.

$$SDC = \frac{\Delta w}{w} = \frac{①}{① + ②} \quad (1)$$

Under cyclic loading, materials exhibit hysteresis, where the stress–strain curve forms a closed hysteresis loop. In the Equation (1), the area of this loop, denoted as $\Delta w$, represents the energy dissipated by the material within one cycle, while w represents the total stored energy throughout the entire cycle process. In this case, the area of $\Delta w$ refers to the shaded area of part ① in the schematic diagram provided in Figure 2d, whereas the area of $w$ corresponds to the total area encompassing both parts ① and ②.

Through calculation, it was observed that for samples subjected to heat treatments at 400 °C for 10 to 60 min and at 450 °C for 10 to 20 min, the values of SDC exhibited approximately linear growth (from 40% to 55%). However, a sudden jump was observed within the 450 °C range at 20 min and 40 min, denoted by red symbols indicating abnormally large SDC values. These anomalies in the two sets of data drew our attention, prompting speculation about a new mechanism possibly involving the introduction of new phases or microstructural organizations causing such a jump.

### *3.3. X-ray Diffraction*

Figure 3a shows the X-ray diffraction (XRD) pattern of as-received NiTi wire. The signal of the whole sample is weak with only one single peak, which means that a strong (110) textile structure exists in the cold-drawn wires. A fine sweep was taken in range from 36–48° and the pattern is shown in Figure 3b, and the broad peak indicates a strong lattice distortion in the as-received NiTi wire. Figure 3c,d shows the fast sweep results for samples heat treated at 400 °C and 450 °C, respectively, for 10, 20, 40, and 60 min. Figure 3e,f shows the corresponding fine sweep results. The peaks corresponding to the B2 austenite phase, B2(110) and B2(211), were observed. Table 1 presents the calculations of the full width at half maximum (FWHM) for the B2(110) peak, which indicates a trend of decreasing FWHM with increasing holding temperature. The FWHM shows a similar trend with aging time, but it is noteworthy that the sample aged at 450 °C for 60 min is an exception, which may be attributed to possible microstructural evolution.

**Table 1.** Calculated FWHM values and 2θ obtained from XRD patterns.

| Samples | 2θ (°) | FWHM (°) |
|---|---|---|
| 400 °C–10 min | 42.508 | 0.741 |
| 400 °C–20 min | 42.470 | 0.661 |
| 400 °C–40 min | 42.486 | 0.652 |
| 400 °C–60 min | 42.525 | 0.646 |
| 450 °C–10 min | 42.260 | 0.516 |
| 450 °C–20 min | 42.485 | 0.491 |
| 450 °C–40 min | 42.603 | 0.347 |
| 450 °C–60 min | 42.529 | 0.360 |
| As-received samples | 43.227 | 2.518 |

Extreme plastic deformation can produce nanocrystalline or amorphous structures in many alloys. Prokoshkin et al. found that the X-ray diffraction peaks progressively converge to 43° with increasing deformation level [19], which is consistent with the results shown in Figure 3b. However, because of this phenomenon, it is challenging to identify the phase composition of the as-received cold-drawn samples. After mid-temperature processing, as shown in Figure 3c,d, only the diffraction peaks of the B2 phase were observed for all the samples. The narrowing peak width shown in Figure 3e,f and Table 1 indicates the release of strong strain, the recovery of grain lattice, and grain growth.

Nevertheless, the XRD outcomes are insufficient to fully elucidate the phase constitution in the thermally treated samples, as the pronounced plastic deformation obscures potential peaks attributable to phases such as martensite B19′ or R phase. Consequently, TEM was employed for further characterization, enabling an in-depth analysis of the possible phase composition and microstructural features within the sample.

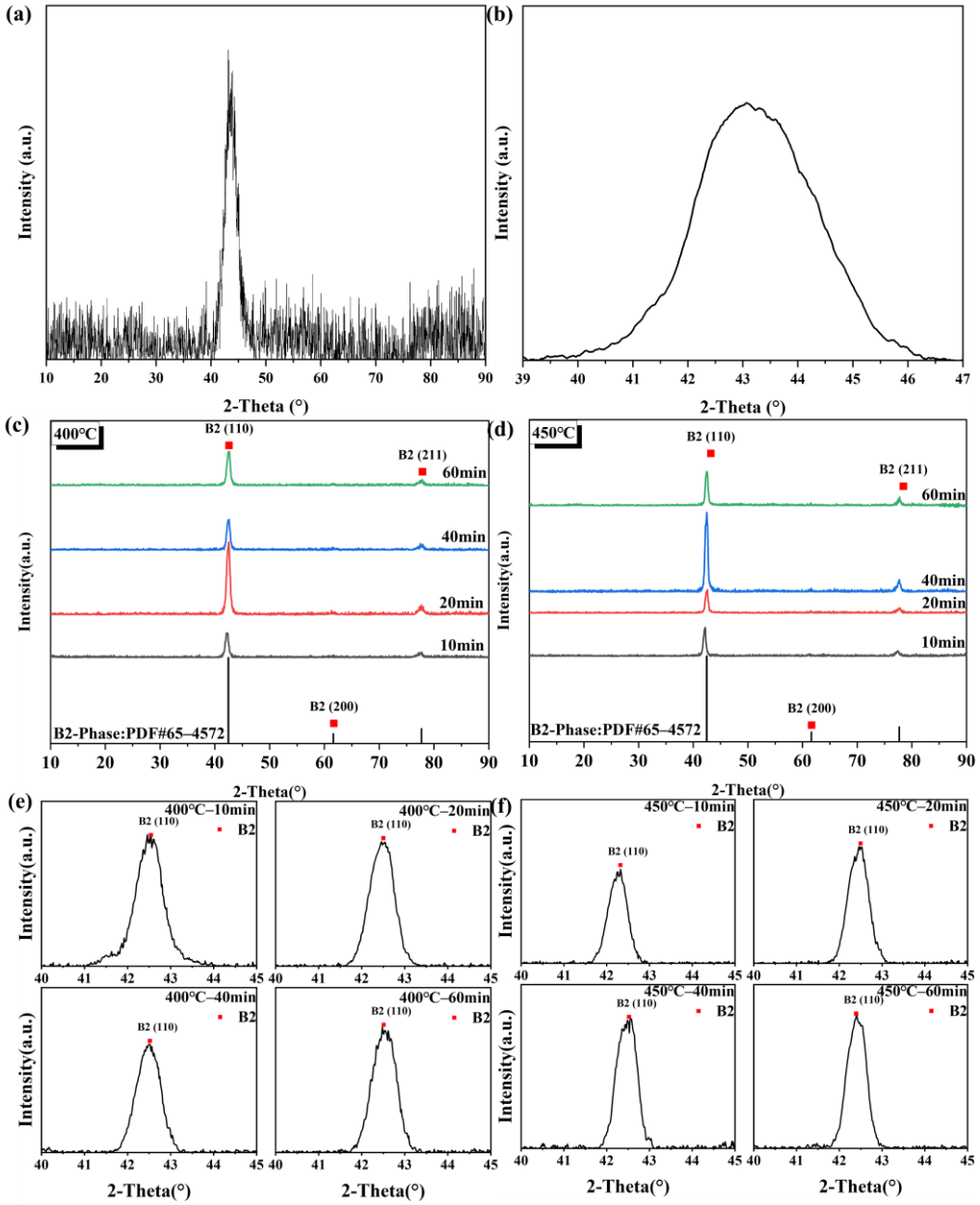


**Figure 3.** XRD patterns of as-received NiTi alloy wires: (**a**) 10–90° wide scanning (**b**) 40–45° fine scanning. XRD patterns of heat-treated samples: (**c**) wide scanning result of #400 °C, (**d**) wide scanning result of #450 °C, (**e**) 40–45° fine scanning result of #400 °C, and (**f**) 40–45° fine scanning result of #450 °C.

### *3.4. TEM Result*

The TEM results are presented in Figure 4. Figure 4a,c show the bright-field images of samples heat treated at 400 °C and 450 °C, respectively, where both samples exhibit fine grains of nanometric dimensions. Figure 4e plots the grain size distribution for both samples, revealing an average grain diameter of 26 nm for the 400 °C–60 min sample and 40 nm for the 450 °C–60 min sample.

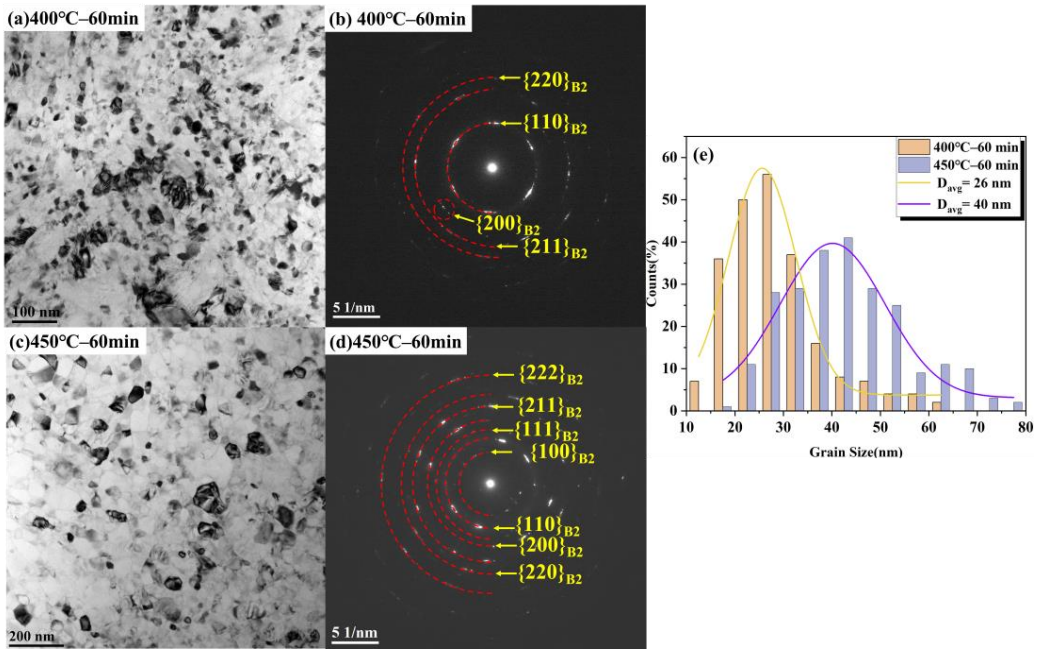


**Figure 4.** (**a**,**c**) TEM images of samples quenched after being held at temperatures of 400 °C and 450 °C, respectively, for 60 min. (**b**,**d**) Selected area electron diffraction (SAED) patterns for the samples treated at 400 °C and 450 °C, respectively, with a selected area diameter of 200 nm. (**e**) Grain size distribution diagram under both heat treatment conditions. Long-axis lengths of more than 300 crystals from each of the two sets of TEM bright-field phase images were measured and the grain distribution with average grain size was obtained.

Figure 4b,d present the selected area electron diffraction (SAED) results corresponding to Figure 4a and 4c, respectively, with the selected areas having a radius of 200 nm. In Figure 4b, the polycrystalline rings characteristic of the austenitic B2 phase could be observed. Figure 4d reveals a slight enhancement in the diffraction intensity of the polycrystalline rings and a greater number of rings assignable to the B2 phase. Nevertheless, SAED analysis could not reveal the presence of phases other than the B2 phase, thereby indicating that the matrix of the 400 °C–60 min and 450 °C–60 min is predominantly composed of the austenitic B2 phase. Kuranova et al. investigated the evolution of phase structures in NiTi alloys following intense torsional plastic deformation upon isothermal annealing within the temperature range of 200–500 °C [20]. They noted that in samples subjected to heat treatment within the 400–500 °C interval, the SAED revealed the presence of distinct diffraction spots corresponding to R phase, B19′ phase, and $Ni_4Ti_3$ nanoprecipitates. The authors proposed that $Ni_4Ti_3$ precipitates formed at grain boundaries, with their content not exceeding 1%. However, despite employing SAED with a probing area significantly larger than the grain size, we still failed to find the evidence for the presence of R phase and other phases, indicating further experimental characterization of phase composition is warranted.

Figure 5a presents a representative HRTEM image of 400 °C–60 min sample, where the red boxed region displays an overlap of multiple lattice fringes, suggesting that multiple phase structures may be present. A fast Fourier transform (FFT) analysis of this region (Figure 5b) reveals that a set of diffraction spots corresponding to the $[\bar{1}11]$ plane of the B2 phase, while the other set belongs to the R phase, the latter of which has been well documented in the literature [13,14,21,22]. Focusing on the R-phase diffraction spots circled in red in Figure 5b, an inverse Fourier transform (IFFT) was performed, yielding the lattice fringes depicted in Figure 5c. It can be seen that there is a high density of edge dislocations in the R-phase lattice structure. We marked the areas where edge dislocations appeared as

accurately as possible in black. According to calculations, the density of edge dislocations is $1.1 \times 10^{21}/m^2$ in this phase.

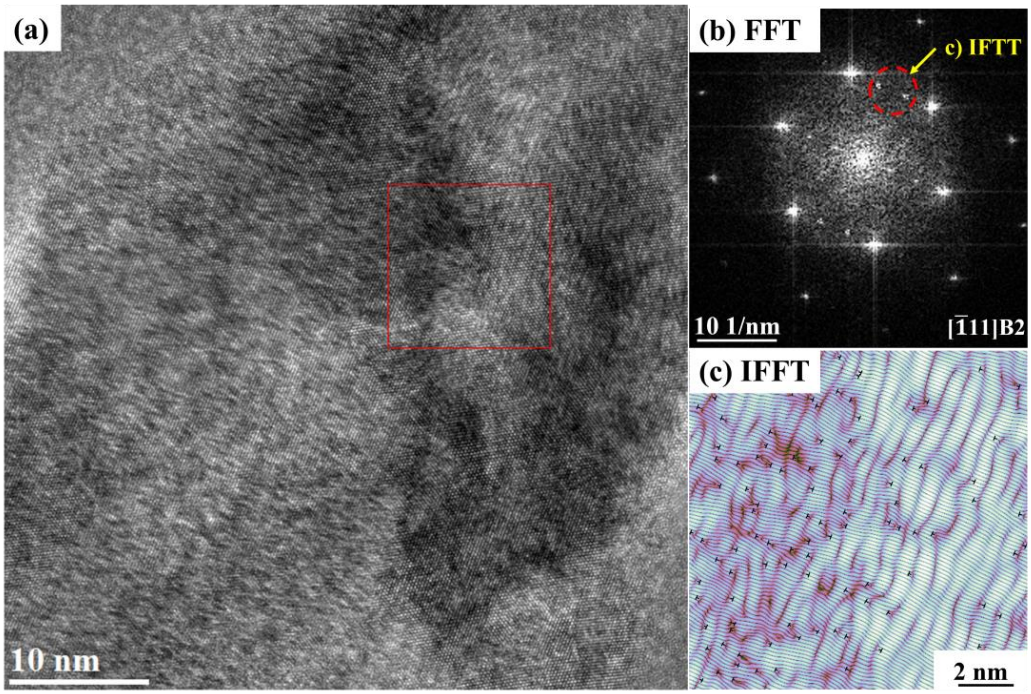


**Figure 5.** (**a**) HRTEM image of 400 °C–60 min sample; (**b**) FFT results obtained from the red frame in (**a**); (**c**) IFFT image of R-phase patterns. Areas where edge dislocations appeared are marked in black.

Similarly, HRTEM characterization was performed on the 450 °C–60 min sample. Figure 6a presents a representative HRTEM image; FFT analysis was applied to the red-framed area, yielding the diffraction spots shown in Figure 6b. In comparison to the diffraction pattern displayed in Figure 5b, a new set of diffraction spots emerges. Yan and Song [13] have previously reported similar diffraction outcomes and proposed that these new spots should be ascribed to variants of the R phase. Furthermore, no diffraction spots indicative of $Ni_4Ti_3$ nanoprecipitates were detected.

Figure 6c, d show the IFFT transformations of the two sets of diffraction spots attributed to the R phase, which we denote as $R_1$ and $R_2$, respectively. Additionally, the $R_2$ phase exhibiting a higher dislocation density than the $R_1$ phase. These nanoscale R-phase variants generate multiple microdomains in the B2 phase matrix, which is similar to the nano-domains reported in [13] These two variants of the R phase give rise to a more uneven distribution of microstress fields.

As shown in Figure 6, the edge dislocations are not very prominent. Therefore, we provided Supplementary Material Figure S1. After calculation, the density of edge dislocations is $6.5 \times 10^{16}/m^2$. Compared to Figure 5c, the density of edge dislocations in samples subjected to 450 °C heat treatment has significantly decreased.

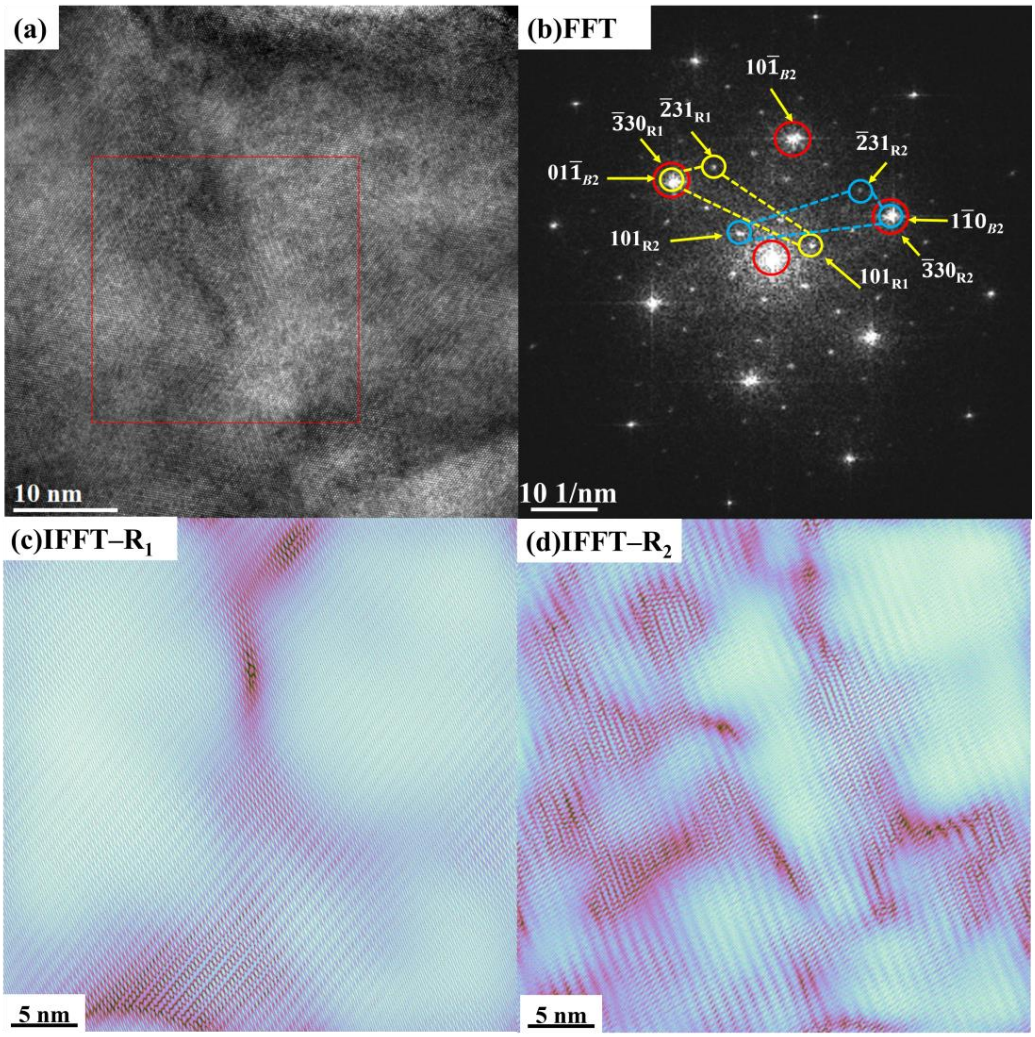


**Figure 6.** (**a**) HRTEM image of the 450 °C–60 min sample; (**b**) FFT results obtained from the red frame in (**a**); (**c**,**d**) IFFT images of $R_1$ and $R_2$.

### *3.5. Internal Friction*

To investigate the formation mechanism of the R phase during cooling, we employed IF technique to examine the dynamic phase transformation process of the samples. The samples were initially held at 90 °C for 10 min to ensure the complete transformation of all R phases and any potential B19′ martensite into the B2 austenite phase. Figure 7a depicts samples subjected to different durations at 400 °C followed by quenching. During the initial cooling stage (from 90 °C to 50 °C), the IF values $Q^{-1}$ are about 0.008,showing the typical IF characteristic of NiTi B2 phase [13,22,23]. With continuous cooling, two distinct peaks, labeled $P_1$ and $P_2$, are observed. The $P_1$ peak is attributed to the phase transformation from the B2 phase to the R phase, according to Song's report [13]. The $P_2$ peak, relatively broad and whose peak position varies with vibration frequency as opposed to $P_1$, is more complex. It should be ascribed to the superposition of the phase transformation peak from R phase to B19′ phase and the relaxation peak of NiTi [13]. However, considering the low-temperature regime associated with this phenomenon, it is out of the scope of present discussion.

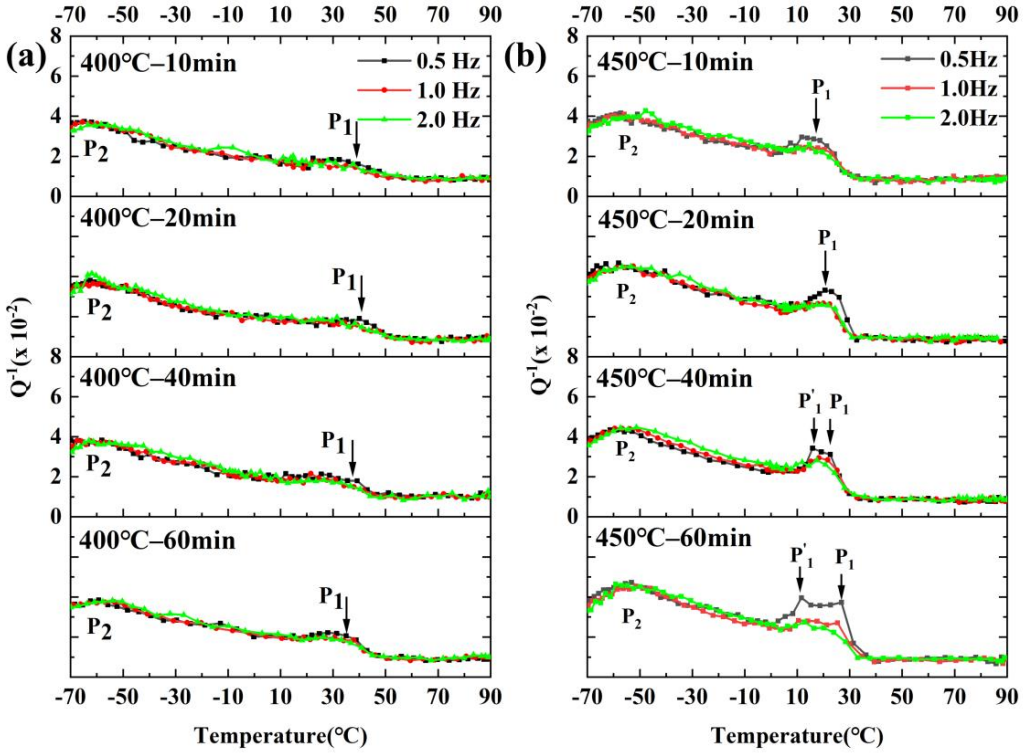


**Figure 7.** IF–temperature curves during cooling run for (**a**) samples quenched after annealing at 400 °C for 10, 20, 40, and 60 min, respectively, and (**b**) samples quenched after annealing at 450 °C for 10, 20, 40, and 60 min, respectively.

Figure 7b shows the temperature-dependent IF curves during cooling run for the samples annealed at 450 °C for 10 min, 20 min, 40 min, and 60 min, respectively. For the IF curve of 450 °C–10 min sample, it exhibits two weak IF peaks as the temperature decreasing, which is same as the curves of 400 °C. The paint peak $P_1$ between 30 °C and 0 °C is frequency-independent, indicating first-order phase transformation trait, which can be attributed to the B2 → R transformation [13,23]. A broad IF peak with faint relaxational characteristic for all samples between −70 °C and 0 °C, and is associated to the thermally activated process of R phase → B19′ as well [13,22,23].

Notably, as the holding time extended, the $P_1$ IF peak progressively broadens and splits, with a new phase transformation peak, designated $P_{1'}$, first emerging in samples annealed for 40 min. This dual peak feature becomes evident in the cooling curve for the 60 min annealed samples, which is particularly evident in the 0.5 Hz curve. Furthermore, with the prolongation of the annealing time, the $P_{1'}$ IF peak shifts conspicuously toward lower temperatures, with the decrease in transformation peak temperature reaching up to 10 °C, while the $P_1$ peak displays a minor tendency to shift towards higher temperature. Frenzel et al. [24] have posited that Ni content has a profound influence on all transformation temperatures in Ni-rich NiTi alloys, such that a mere 0.1 at% change in Ni composition within the atomic ratio range of 50.0 to 51.2 at% for NiTi alloys can lead to a 10 °C drop in transformation temperatures. Unfortunately, Frenzel's study did not encompass investigations into the transformation temperatures of the R phase. Nonetheless, Urbina et al. [17] and Héraud et al. [18] have each suggested that the R-phase transformation represents a variant of the martensitic transformation, acting as an intermediate state in the B2 to B19′ transformation process. Drawing inference from these conclusions, we can posit that the $P_{1'}$ peak should also be attributed to the transformation from B2 to R phase, implying that our IF experiments have captured the dynamic transformation processes of two R-phase variants.

Finally, our experimental findings still entail two issues worthy of discussion. Firstly, past reports [11,12,25] on the R phase often emphasize that the introduction of $Ni_4Ti_3$

nanoprecipitates through low- or intermediate-temperature aging heat treatments facilitates the formation of the R phase. However, none of our experimental results could confirm the presence of either $Ni_4Ti_3$ or $Ti_2Ni$ nanoprecipitates. Consequently, the following question arises: What is the underlying cause for the generation of the R phase in our case? Takashi [26] pointed that the R phase can nucleate from single dislocations and other defects. Song [13] demonstrated that the generation of R-phase variants was promoted by short-range ordering of Ni atoms under mid-temperature aging. Huo observed segregation of Ni elements in samples subjected to low-temperature aging and, through molecular dynamics calculations, concluded that R-phase transformation is initiated when strain fluctuations exceed ±3% [14]. Based on the experimental results presented above and in comparison with previous reports, particularly considering the uneven distribution of dislocation densities revealed in Figure 6c,d, we can infer that the R phase observed in our experiments is induced by a non-uniform stress field resulting from this irregular distribution of edge dislocations.

Additionally, the $P_1$ and $P_{1'}$ IF peaks appear to correlate with the two R-phase variants depicted in Figure 6c and 6d, respectively. Given that the quenching temperature of the samples is 18 °C, which is higher than the temperature of the $P_1$ peak yet lower than that of the $P_{1'}$ peak, the phase composition of the quenched samples would logically contain a significantly greater volume fraction of the R phase corresponding to the $P_1$ peak than that related to the $P_{1'}$ peak. Building on the above inferences, we contend that the $P_1$ IF peak should be associated with the $R_2$ phase diffraction spots shown in Figure 6d, while the $P_{1'}$ peak aligns with the $R_1$ phase diffraction spots presented in Figure 6c. Lastly, we realize that a segregation of Ni elements has occurred within the NiTi B2 matrix, leading to microregions with varying Ni contents due to the rapid heat treatment regimen employed.

## 4. Conclusions

Mid-temperature rapid heat treatment process was employed to fabricate NiTi alloys containing multiple R-phase variants, characterized using XRD, TEM, and internal friction techniques, leading to the following findings:

(1) Within the heat treatment window of 400 to 450 °C, a holding period of less than one hour followed by quenching yields NiTi nano-crystalline alloys incorporating a nanoscale R phase. TEM results confirmed that this process avoids the formation of nanoprecipitates like $Ni_4Ti_3$, thereby preserving a sufficient Ni content in the NiTi matrix.

(2) The appearance of the R phase is attributed to an unevenly distributed stress field, which is different from the traditionally mechanism involving nanoprecipitates by mid-temperature aging.

(3) Utilizing the internal friction technique, the dynamic splitting of a single R phase into two distinct R-phase variants was observed, indicating Ni segregation within the B2 matrix. These two R-phase variants partition the B2 austenite phase into multiple microdomains with varying Ni concentrations, with the enrichment and depletion of Ni in these microdomains driving this observed dynamic phenomenon.

**Supplementary Materials:** The following supporting information can be downloaded at: https://www.mdpi.com/article/10.3390/cryst14050476/s1, Figure S1: (a) Another HRTEM image, (b) the FFT result of red box in (a), (c) the IFFT result of $R_1$ in (b) and (d) the IFFT result of $R_2$ in (b).

**Author Contributions:** Conceptualization, Y.X., J.C. and W.J.; methodology, Y.X.; validation, Y.X., J.C. and X.W. (Xinggang Wang); formal analysis, Y.X., J.C. and X.W. (Xinggang Wang); investigation, Y.X.; data curation, Y.X. and J.C.; writing—original draft preparation, Y.X.; writing—review and editing, W.J. and M.S.; funding acquisition, W.J. and X.W. (Xianping Wang). All authors have read and agreed to the published version of the manuscript.

**Funding:** This work was supported by the Strategic Priority Research Program of the Chinese Academy of Sciences [No. XDB0470303], the National Natural Science Foundation of China [No. 52101159, 52173303], and the HFIPS Director's Fund [No. YZJJ-GGZX-2022-01].

**Data Availability Statement:** The data supporting the conclusions of this article will be made available by the authors on request.

**Conflicts of Interest:** The authors declare no conflicts of interest.

## References


1. Khalili, V.; Naji, H. Developing a Mechanochemical Surface Pretreatment to Increase the Adhesion Strength of Hydroxyapatite Electrophoretic Coating on the NiTi Alloy as a Bone Implant. *Surf. Coat. Technol.* **2020**, *397*, 125985. [CrossRef]
2. Zhu, S.L.; Yang, X.J.; Chen, M.F.; Li, C.Y.; Cui, Z.D. Effect of Porous NiTi Alloy on Bone Formation: A Comparative Investigation with Bulk NiTi Alloy for 15 Weeks in Vivo. *Mater. Sci. Eng. C* **2008**, *28*, 1271–1275. [CrossRef]
3. Wu, G.; Li, L.; Sun, M.; Wang, Y.; Luo, F.; Zhang, Q.; Liu, R.; Chen, Z.; Yao, J. Microstructural Evolution and Biological Properties of PEO Coating on SLM-Prepared NiTi Alloy. *Surf. Coat. Technol.* **2023**, *452*, 129065. [CrossRef]
4. Patel, S.K.; Behera, B.; Swain, B.; Roshan, R.; Sahoo, D.; Behera, A. A Review on NiTi Alloys for Biomedical Applications and Their Biocompatibility. *Mater. Today Proc.* **2020**, *33*, 5548–5551. [CrossRef]
5. Hartl, D.J.; Lagoudas, D.C. Aerospace Applications of Shape Memory Alloys. *Proc. Inst. Mech. Eng. Part G J. Aerosp. Eng.* **2007**, *221*, 535–552. [CrossRef]
6. Saburi, T.; Nenno, S.; Fukuda, T. Crystal Structure and Morphology of the Metastable X Phase in Shape Memory Ti-Ni Alloys. *J. Common Met.* **1986**, *125*, 157–166. [CrossRef]
7. Waitz, T.; Kazykhanov, V.; Karnthaler, H.P. Martensitic Phase Transformations in Nanocrystalline NiTi Studied by TEM. *Acta Mater.* **2004**, *52*, 137–147. [CrossRef]
8. McCormick, P.G.; Liu, Y. Thermodynamic Analysis of the Martensitic Transformation in NiTi—II. Effect of Transformation Cycling. *Acta Metall. Mater.* **1994**, *42*, 2407–2413. [CrossRef]
9. Wang, X.B.; Verlinden, B.; Van Humbeeck, J. R-Phase Transformation in NiTi Alloys. *Mater. Sci. Technol.* **2014**, *30*, 1517–1529. [CrossRef]
10. Tirry, W.; Schryvers, D. Linking a Completely Three-Dimensional Nanostrain to a Structural Transformation Eigenstrain. *Nat. Mater.* **2009**, *8*, 752–757. [CrossRef]
11. Khalil-Allafi, J.; Dlouhy, A.; Eggeler, G. Ni4Ti3-Precipitation during Aging of NiTi Shape Memory Alloys and Its Influence on Martensitic Phase Transformations. *Acta Mater.* **2002**, *50*, 4255–4274. [CrossRef]
12. Tirry, W.; Schryvers, D. Quantitative Determination of Strain Fields around $Ni_4Ti_3$ Precipitates in NiTi. *Acta Mater.* **2005**, *53*, 1041–1049. [CrossRef]
13. Song, Y.; Jin, M.; Han, X.; Wang, X.; Chen, P.; Jin, X. Microstructural Origin of Ultrahigh Damping Capacity in $Ni_{50.8}Ti_{49.2}$ Alloy Containing Nanodomains Induced by Insufficient Annealing and Low-Temperature Aging. *Acta Mater.* **2021**, *205*, 116541. [CrossRef]
14. Huo, X.; Chen, P.; Lahkar, S.; Jin, M.; Han, X.; Song, Y.; Wang, X. Occurrence of the R-Phase with Increased Stability Induced by Low Temperature Precipitate-Free Aging in a $Ni_{50.9}Ti_{49.1}$ Alloy. *Acta Mater.* **2022**, *227*, 117688. [CrossRef]
15. Bojda, O.; Eggeler, G.; Dlouhý, A. Precipitation of $Ni_4Ti_3$-Variants in a Polycrystalline Ni-Rich NiTi Shape Memory Alloy. *Scr. Mater.* **2005**, *53*, 99–104. [CrossRef]
16. Jiang, S.; Zhang, Y.; Zhao, Y.; Liu, S.; Hu, L.; Zhao, C. Influence of $Ni_4Ti_3$ Precipitates on Phase Transformation of NiTi Shape Memory Alloy. *Trans. Nonferrous Met. Soc. China* **2015**, *25*, 4063–4071. [CrossRef]
17. Urbina, C.; De la Flor, S.; Gispert-Guirado, F.; Ferrando, F. Quantitative XRD Analysis of the Evolution of the TiNi Phase Transformation Behaviour in Relation to Thermal Treatments. *Intermetallics* **2010**, *18*, 1632–1641. [CrossRef]
18. Héraud, L.; Castany, P.; Ijaz, M.F.; Gordin, D.-M.; Gloriant, T. Large-Strain Functional Fatigue Properties of Superelastic Metastable β Titanium and NiTi Alloys: A Comparative Study. *J. Alloys Compd.* **2023**, *953*, 170170. [CrossRef]
19. Prokoshkin, S.D.; Brailovski, V.; Korotitskiy, A.V.; Inaekyan, K.E.; Glezer, A.M. Specific Features of the Formation of the Microstructure of Titanium Nickelide upon Thermomechanical Treatment Including Cold Plastic Deformation to Degrees from Moderate to Severe. *Phys. Met. Metallogr.* **2010**, *110*, 289–303. [CrossRef]
20. Kuranova, N.N.; Gunderov, D.V.; Uksusnikov, A.N.; Luk'yanov, A.V.; Yurchenko, L.I.; Prokof'ev, E.A.; Pushin, V.G.; Valiev, R.Z. Effect of Heat Treatment on the Structural and Phase Transformations and Mechanical Properties of TiNi Alloy Subjected to Severe Plastic Deformation by Torsion. *Phys. Met. Metallogr.* **2009**, *108*, 556–568. [CrossRef]
21. Liang, X.; Xiao, F.; Chen, H.; Li, Z.; Jin, X.; Fukuda, T. Growth of B2 Parent Phase Grain Assisted by Martensitic Transformation in a Nanocrystalline Ti-50.8Ni (at.%) Shape Memory Alloy. *Scr. Mater.* **2019**, *159*, 37–40. [CrossRef]
22. Jin, M.; Song, Y.; Wang, X.; Chen, P.; Pang, G.; Jin, X. Ultrahigh Damping Capacity Achieved by Modulating R Phase in $Ti_{49.2}Ni_{50.8}$ Shape Memory Alloy Wires. *Scr. Mater.* **2020**, *183*, 102–106. [CrossRef]
23. Lin, H.C.; Wu, S.K.; Chou, T.S. Aging Effect on the Low Temperature Internal Friction Relaxation Peak in a $Ti_{49}Ni_{51}$ Alloy. *J. Alloys Compd.* **2003**, *355*, 90–96. [CrossRef]
24. Frenzel, J.; George, E.P.; Dlouhy, A.; Somsen, C.; Wagner, M.F.-X.; Eggeler, G. Influence of Ni on Martensitic Phase Transformations in NiTi Shape Memory Alloys. *Acta Mater.* **2010**, *58*, 3444–3458. [CrossRef]

25. Zhu, J.; Wu, H.-H.; Wu, Y.; Wang, H.; Zhang, T.; Xiao, H.; Wang, Y.; Shi, S.-Q. Influence of $Ni_4Ti_3$ Precipitation on Martensitic Transformations in NiTi Shape Memory Alloy: R Phase Transformation. *Acta Mater.* **2021**, *207*, 116665. [CrossRef]
26. Fukuda, T.; Saburi, T.; Doi, K.; Nenno, S. Nucleation and Self-Accommodation of the R-Phase in Ti–Ni Alloys. *Mater. Trans. JIM* **1992**, *33*, 271–277. [CrossRef]